

# Angular momentum transport via gravitational instability in the Elias 2-27 disc

C. Longarini<sup>1,2</sup>, G. Lodato<sup>2</sup>, C. J. Clarke<sup>1</sup>, J. Speedie<sup>3</sup>, T. Paneque-Carreño<sup>4,7</sup>, E. Arrigoni<sup>2</sup>, P. Curone<sup>2</sup>, C. Toci<sup>4</sup>, C. Hall<sup>5,6</sup>

<sup>1</sup> Institute of Astronomy, University of Cambridge, Madingley Road, Cambridge, CB3 0HA, United Kingdom  
e-mail: c12000@cam.ac.uk

<sup>2</sup> Dipartimento di Fisica, Università degli Studi di Milano, Via Celoria 16, Milano, 20133, Italy

<sup>3</sup> Department of Physics & Astronomy, University of Victoria, Victoria, BC V8P 5C2, Canada

<sup>4</sup> European Southern Observatory, Karl-Schwarzschild-Strasse 2, D-85748 Garching bei Munchen, Germany

<sup>5</sup> Department of Physics and Astronomy, The University of Georgia, Athens, GA 30602, USA

<sup>6</sup> Center for Simulational Physics, The University of Georgia, Athens, GA 30602, USA

<sup>7</sup> Leiden Observatory, Leiden University, P.O. Box 9513, NL-2300 RA Leiden, the Netherlands

Received ; accepted

## ABSTRACT

Gravitational instability is thought to be one of the main drivers of angular momentum transport in young protoplanetary discs. The disc around Elias 2-27 offers a unique example of gravitational instability at work. It is young and massive, displaying two prominent spiral arms in dust continuum emission and global non-axisymmetric kinematic signatures in molecular line data.

In this work, we used archival ALMA observations of <sup>13</sup>CO line emission to measure the efficiency of angular momentum transport in the Elias 2-27 system through the kinematic signatures generated by gravitational instability, known as 'GI wiggles'. Assuming the angular momentum is transported by the observed spiral structure and leveraging previously-derived dynamical disc mass measurements, the amount of angular momentum transport we found corresponds to an  $\alpha$ -viscosity of  $\alpha = 0.038 \pm 0.018$ . This value implies an accretion rate onto the central star of  $\log_{10} \dot{M}_* = -6.99 \pm 0.17 M_\odot/\text{yr}$ , which reproduces the one observed value of  $\log_{10} \dot{M}_{*,\text{obs}} = -7.2 \pm 0.5 M_\odot/\text{yr}$  very well. The excellent agreement we have found serves as further proof that gravitational instability is the main driver of angular momentum transport acting in this system.

**Key words.** protoplanetary discs – gravitational instability – planet formation

## 1. Introduction

Elias 2-27 is a young ( $\sim 0.5\text{Myr}$ ,  $M_* = 0.46M_\odot$ ) M0 star (Andrews et al. 2009) located at a distance of 116 pc (Gaia Collaboration et al. 2018) in the  $\rho$ -Oph star forming region, hosting a likely gravitationally unstable disc. The circumstellar disc shows two large-scale trailing spiral arms in dust continuum emission (Pérez et al. 2016), whose origins were first attributed to gravitational instability, due to the high dust mass. An estimate of the total dynamical mass of the disc has been provided by Veronesi et al. (2021),  $M_d = 0.08 \pm 0.04M_\odot$ , implying a disc-to-star mass ratio of 17%. Meru et al. (2017) performed three-dimensional (3D) numerical SPH simulations to investigate the origin of the spiral structure: by comparing gravitational instability and internal and external companion scenarios, they found that GI best reproduces the observed morphology. Similar results have also been found by Hall et al. (2018). In addition, due to its high brightness, Elias 2-27 has become part of the the DSHARP sample (Andrews et al. 2018), allowing for more thorough studies of its dust morphology. Huang et al. (2018) characterised annular substructures in the discs within the DSHARP sample, finding that Elias 2-27 has a gap at  $\sim 70\text{au}$ . Even though the main focus of the DSHARP program was dust emission, also kinematic data on CO isotopologues were collected. Pinte et al. (2020) found complex kinematic features in the Elias 2-27 system, showing perturbations to the velocity field. However, due to the low reso-

lution of the data, a detailed analysis was not possible. Paneque-Carreño et al. (2021) presented new data on this system and conducted a detailed analysis of the morphology and the kinematics. Global perturbations in the velocity field of <sup>13</sup>CO and C<sup>18</sup>O were found and their morphology follows the shape of the spiral, consistent with kinematic signatures of GI induced density waves, or GI Wiggles (Hall et al. 2020; Longarini et al. 2021; Terry et al. 2022). From the same dataset, Veronesi et al. (2021) studied the rotation curve and obtained the previously mentioned disc mass, by measuring the super-Keplerian contribution of the disc self-gravity.

In this letter, we study the GI Wiggle in Elias 2-27. Thanks to the disc mass estimate provided by Veronesi et al. (2021), we have been able to constrain the amount of angular momentum transported throughout the disc. In Section 2, we discuss the theoretical framework we use in this Letter. In Section 3, we present the dataset and the analysis. In Section 4, we discuss the results and in Section 5 we draw our conclusions.

## 2. Gravitational instability in protoplanetary discs

The onset of gravitational instability is determined by the Toomre parameter

$$Q = \frac{c_s \kappa}{\pi G \Sigma}, \quad (1)$$

where  $\kappa$  is the epicyclic frequency, which (for a Keplerian disc) is just the Keplerian frequency,  $\Omega_k$ ;  $\Sigma$  is the surface density; and  $c_s$  the sound speed. Essentially,  $Q$  measures the strength of stabilising terms (e.g. pressure and rotation, at the numerator) compared to destabilising ones (e.g. self-gravity, at the denominator). A protoplanetary disc is marginally unstable when  $Q \simeq 1$ : in this regime, the disc develops a spiral structure and, by means of shocks, this leads to energy dissipation and heating. One of the most important consequences of gravitational instability is its ability to drive angular momentum transport throughout the disc, and therefore induce accretion onto the central object (Lynden-Bell & Kalnajs 1972).

### 2.1. Gravito-turbulence and transport of angular momentum

A disc is in the gravito-turbulent regime when its angular momentum transport is driven by gravitational instability. In this context, the  $R\phi$  component of the vertically integrated stress tensor can be written as:

$$T_{R\phi} = \int \left\langle \frac{g_R g_\phi}{4\pi G} \right\rangle dz, \quad (2)$$

where  $g_R, g_\phi$  are the radial and azimuthal component of the perturbed self-gravitating field, and the brackets indicate azimuthal averaging. To this stress, it is necessary to also add the induced Reynolds stress, given by:

$$T_{R\phi} = \Sigma \langle \delta v_R \delta v_\phi \rangle, \quad (3)$$

where  $\delta v_R$  and  $\delta v_\phi$  are the perturbed fluid velocities (Balbus & Papaloizou 1999). In the classic viscous scenario, this term is responsible for angular momentum transport in the accretion disc. The Shakura and Sunyaev  $\alpha$ -prescription (Shakura & Sunyaev 1973) relates the stress tensor to the local disc pressure

$$T_{R\phi} = \alpha \Sigma c_s^2 \frac{d \log \Omega}{d \log R}, \quad (4)$$

where, for a Keplerian disc,  $d \log \Omega_k / d \log R = -3/2$ . It is possible to show that the transport of energy and angular momentum through the propagation of the GI spiral density waves can be divided into two parts (Toomre 1969; Shu 1970): a non-local term and a viscous-like term. Since the non-local term is important only for very high disc-to-star mass ratios,  $M_d/M_\star \gtrsim 0.5$  (Lodato & Rice 2005), gravitationally unstable protostellar discs essentially behave as  $\alpha$ -discs (Lodato & Rice 2004; Forgan et al. 2011).

To characterise the transport of angular momentum through spiral density waves, we need to rely on numerical simulations of gravitationally unstable discs (Cossins et al. 2009). Usually in numerical simulations of gravitationally unstable discs, the  $\beta$  cooling framework is adopted (Gammie 2001). We suppose that the disc is cooling with a rate per unit mass of:

$$\dot{q}^- = -\frac{e}{t_{\text{cool}}}, \quad (5)$$

where  $e = c_s^2 / \gamma(\gamma - 1)$  is the internal energy per unit mass, with the adiabatic index  $\gamma = 5/3$ , and the cooling time is defined in terms of the dynamical one:  $t_{\text{cool}} = \beta \Omega^{-1}$ . In the absence of external heating mechanisms, an initially stable hot disc ( $Q \gg 1$ ) will cool down, eventually reaching the marginally stable state ( $Q = 1$ ). At this point, gravitational instability turns on: the disc develops a spiral structure that, by means of compression and shocks, leads to efficient energy dissipation and heating. In this

sense, the  $Q$ -stability condition acts as a thermostat so that heating turns on only if the system is sufficiently cold, keeping it in a marginally stable state (Kratter & Lodato 2016). In this regime, namely, thermal saturation, the cooling is completely balanced by heating provided by the shocks, and the amplitude of spiral perturbations saturates at a fixed value, according to Cossins et al. (2009):

$$\left( \frac{\delta \Sigma}{\Sigma} \right) = \left[ \frac{2}{\epsilon \beta \gamma (\gamma - 1)} \frac{1}{\mathcal{M} \tilde{\mathcal{M}}} \right]^{1/2} = \chi \beta^{-1/2}, \quad (6)$$

where  $\epsilon$  is the heating factor,  $\mathcal{M}$  and  $\tilde{\mathcal{M}}$  are the Mach numbers relative to the radial phase speed and Doppler-shifted radial phase speed of the wave: respectively,  $m\Omega_p/k$  and  $m(\Omega - \Omega_p)/k$ , with  $\Omega_p$  as the spiral pattern frequency. Cossins et al. (2009) showed through numerical simulations that the relevant scaling of the spiral density perturbation is  $\beta^{-1/2}$  and the other terms of the order of unity. For this reason, we introduce  $\chi$ , which is of the order of unity. In the thermal saturation regime, the transport of angular momentum provided by gravitational instability is described within an  $\alpha$ -framework (Kratter & Lodato 2016):

$$\alpha_{\text{GI}} = \left| \frac{d \log \Omega}{d \log R} \right|^{-2} \frac{1}{\gamma(\gamma - 1)\beta}. \quad (7)$$

Combining Eqs. (7) and (6), we obtain the relationship between the amplitude of the density wave and the amount of angular momentum

$$\frac{\delta \Sigma}{\Sigma} = \frac{3\chi}{2} \sqrt{\gamma(\gamma - 1)} \alpha_{\text{GI}}^{1/2}, \quad (8)$$

where the last equation is valid for a Keplerian disc. In the following, we assume that the constant of proportionality is  $\chi = 1$ , which is well justified by numerical simulations (Cossins et al. 2009).

### 2.2. Kinematic signatures of gravitational instability

Kinematics offers a unique opportunity to quantify the transport of angular momentum in a gravitationally unstable disc. Indeed, when there is a spiral density wave, also the velocity field is affected. Hall et al. (2020) predicted that a disc undergoing such instability has clear kinematic signatures in molecular line observations across the entire disc azimuth and radius, called ‘GI wiggles’. Longarini et al. (2021) provided an analytical model to describe such kinematic signatures, implemented in the publicly available code GIGGLE<sup>1</sup>. Under the hypothesis of thin disc, in a marginally unstable regime ( $Q = 1$ ) and in thermal saturation, the amplitude of the velocity perturbation increases with the disc-to-star mass ratio ( $M_d/M_\star$ ), as has also been described with numerical simulations (Terry et al. 2022), and which is proportional to the cooling factor,  $\beta^{-1/2}$ . However, from the analysis carried out in Longarini et al. (2021), the actual quantity that determines the amplitude of the velocity perturbations ( $\delta u_R, \delta u_\phi$ ) is the amplitude of the spiral density wave,  $\delta \Sigma / \Sigma$ . This quantity is intrinsically linked to the efficiency of angular momentum transported by the spiral, which can be described within an  $\alpha$ -viscosity framework through Eq. (7). Thus, it is possible to constrain the value of  $\alpha_{\text{GI}}$  from the amplitude of the wiggle. Rewriting the velocity perturbations (Eq. 22 of Longarini et al. (2021)) as a function of  $\alpha_{\text{GI}}$ , we obtain:

$$\delta u_R = 3im\alpha_{\text{GI}}^{1/2} \sqrt{\gamma(\gamma - 1)} \left( \frac{M_d}{M_\star} \right)^2 u_k, \quad (9)$$

<sup>1</sup> <https://doi.org/10.5281/zenodo.10205110>

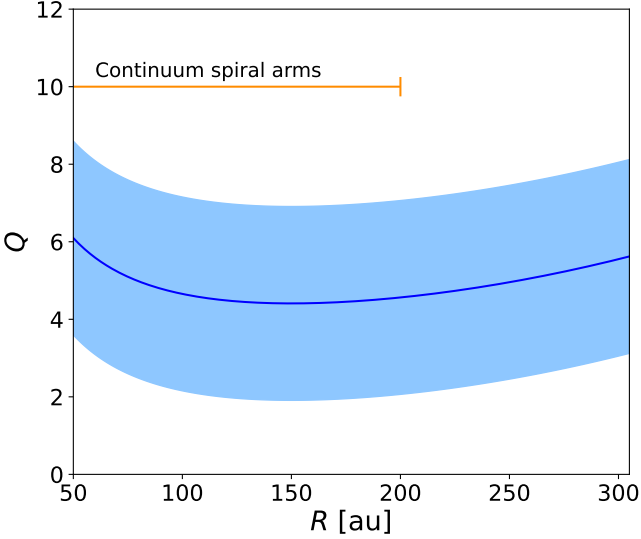


**Fig. 1.** Toomre profile of Elias 2-27, where the shaded region indicates the uncertainties on the disc and star mass from Veronesi et al. (2021).

$$\delta u_\phi = -\frac{3i\alpha_{\text{GI}}^{1/2}}{4} \sqrt{\gamma(\gamma-1)} \left(\frac{M_d}{M_\star}\right) u_k. \quad (10)$$

The final expressions for the velocity field are:

$$u_\phi(R, \phi) = R\Omega + \Re \left[ \delta u_\phi(R) e^{i(m\phi + \psi)} \right] = R\Omega - |\delta u_\phi(R)| \sin(m\phi + \psi), \quad (11)$$

$$u_R(R, \phi) = \Re \left[ \delta u_R(R) e^{i(m\phi + \psi)} \right] = -|\delta u_R(R)| \sin(m\phi + \psi). \quad (12)$$

### 3. Gravitational instability in Elias 2-27

#### 3.1. Toomre parameter

Veronesi et al. (2021) estimated the dynamical mass of Elias 2-27 from  $^{13}\text{CO}$  and  $\text{C}^{18}\text{O}$  rotation curves, and found  $M_\star = 0.46M_\odot \pm 0.03$  and  $M_d = 0.08 \pm 0.04M_\odot$ . In their fit, they used a self-similar surface density given by

$$\Sigma = \frac{M_d}{2\pi(200\text{au})^2} \left(\frac{R}{200\text{au}}\right)^{-1} \exp\left[-\frac{R}{200\text{au}}\right], \quad (13)$$

where the scale radius has been fixed to  $R_c = 200\text{au}$ . As for the thermal structure, they assumed a vertically isothermal disc with  $T(R) = 20(R/60\text{au})^{0.5}\text{K}$  taken from Pérez et al. (2016), which corresponds to a sound speed of  $c_s = 281\text{m/s}(R/60\text{au})^{-0.25}$ . With this information, it is possible to compute the Toomre parameter profile for Elias 2-27, as displayed in Fig. 1. Despite not being exactly  $Q = 1$ , the Toomre profile is close enough to the critical threshold to consider gravitational instability to be significant. In addition, we are not considering uncertainties on  $T(R)$ , that can impact on the  $Q$ -parameter estimate. Finally, we know that the disc shows non-axisymmetric features in gas and dust, making the azimuthally averaged Toomre profile solely an approximation of the actual value.

#### 3.2. Dataset

In this work, we use the  $^{13}\text{CO } J = 3 - 2$  datacube presented in Paneque-Carreño et al. (2021). The images have been obtained with a robust parameter of 0.5, resulting in a beam size of  $0.26'' \times 0.25''$  for the  $^{13}\text{CO}$  and a spectral resolution of  $\Delta v = 111\text{m/s}$ . Further details of the observations and reduction can be found in Paneque-Carreño et al. (2021). In this work, we use a Gaussian velocity map obtained with BETTERMOMENTS (Teague & Foreman-Mackey 2018). The code also returns a map of the errors on the velocity field (Teague 2019). In the analysis, we masked the emission coming from the first two beams ( $\sim 50\text{au}$ ).

#### 3.3. Model of the GI wobble of Elias 2-27

In the analytical model for the GI wobble of Longarini et al. (2021), the amplitude of the velocity perturbations is determined by the disc to star mass ratio and the cooling factor. There is a degeneracy between the two quantities; however, in the case of Elias 2-27 the value of the disc to star mass ratio is known (Veronesi et al. 2021). Longarini et al. (2021) showed that the amplitude of the wobble in the PP (position-position) space scales as  $\beta^{-1/2}$  (i.e.  $\alpha_{\text{GI}}^{1/2}$ ), and they proposed this relationship as a way to constrain this unknown parameter. In this paragraph, we study the wobble in the PV (position-velocity) space, as done in Speedie et al. (2024, submitted). We consider the observed velocity field:

$$u_{\text{obs}}(R, \phi) = \left[ u_\phi(R, \phi) \cos \phi + u_R(R, \phi) \sin \phi \right] \sin i, \quad (14)$$

where  $u_\phi$  and  $u_R$  are described by the model presented in Eqs. (11) and (12) and  $i$  is the disc inclination. We compute the variation of velocity along the semi-minor axis of the disc (i.e.  $\phi = -\pi/2$ ), because along this axis only the radial velocity contributes to the observed velocity field

$$u_{\text{obs}}(R, -\pi/2) = -2m\beta^{-1/2} \left(\frac{M_d(R)}{M_\star}\right)^2 u_k \sin(\psi(R) + \psi_0), \quad (15)$$

where  $\psi(R)$  is the phase function of the spiral that is given by

$$\frac{d\psi}{dR} = \frac{m}{R \tan \alpha_p}, \quad (16)$$

with  $\alpha_p$  being the pitch angle of the spiral and  $\psi_0$  is just a phase shift. We suppose that the pitch angle is constant over the radial extent of the disc, that is well justified for GI spirals (Cossins et al. 2009). We note that the last equation can be written as a function of  $\alpha_{\text{GI}}$  as:

$$u_{\text{obs}}(R, -\pi/2) = -3m\alpha_{\text{GI}}^{1/2} \sqrt{\gamma(\gamma-1)} \left(\frac{M_d(R)}{M_\star}\right)^2 u_k \sin(\psi(R) + \psi_0). \quad (17)$$

We then extract the PV wobble by cutting along the semi-minor axis and considering just the southern part of the disc, on account of cloud contamination (Paneque-Carreño et al. 2021). The errors on the velocity are returned by (Teague & Foreman-Mackey 2018) as shown in figure 2. The disc and spiral parameters we use are taken from literature, namely,  $M_\star = 0.46M_\odot$ ,  $M_d = 0.08M_\odot$ ,  $R_c = 200\text{au}$  (Veronesi et al. 2021),  $\alpha_p = 13^\circ$ ,  $i = 56.2^\circ$ , PA =  $118.8^\circ$  (Paneque-Carreño et al. 2021), and  $m = 2$ . Hence, the only free parameters in Eq. (17) are  $\alpha_{\text{GI}}$  and  $\psi_0$ . To fit the curve to the data, we used the method of nonlinear

least squares implemented in `SCIPY` (Virtanen et al. 2020). While the spiral pattern in the continuum extends to approximately 200au, non-axisymmetric kinematic signatures in the gas emission are observable across the entire radial extent of the disk. Hence, in the fitting procedure, we analysed the signal up to the outer edge of the disc. The best-fit values are  $\alpha_{\text{GI}} = 0.038 \pm 0.018$  and  $\psi_0 = 43^\circ \pm 1^\circ$ . The value of  $\alpha_{\text{GI}}$  corresponds to a  $\beta = 10.5$ , meaning that the cooling time of the system is approximately ten times the dynamical one. We estimated the error on  $\alpha_{\text{GI}}$  propagating the uncertainties on star and disc masses<sup>2</sup>.

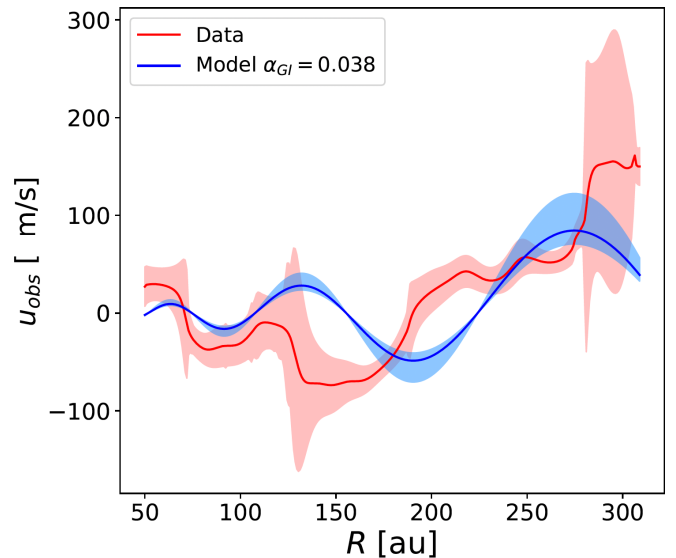
Figure 2 shows the comparison between the extracted PV wiggle from  $^{13}\text{CO}$  data and the model that best describes the data. By comparing the model and the data, we observe that the overall shape of the perturbation is well reproduced. However, it appears that there is a radial shift between the two curves. This effect can be attributed to the fact that in the analytical model, we assume that a single spiral mode is present, with  $m = 2$ , and we also suppose that the perturbation wave-number,  $k$ , is the most unstable ( $k_{\text{uns}}$ ). While the  $m = 2$  mode, with  $k = k_{\text{uns}}$  may be the dominant one, determining the overall morphology of the spiral, this does not prevent the presence of additional lower amplitude modes that will interfere with the dominant one and thus create a more complex pattern than the purely sinusoidal one that we assume here. The scope of this work is to find the amount of stress generated by gravitational instability; hence, we are interested in the amplitude of the wiggle, not in the whole shape. For this reason, the additional lower amplitude modes are not a concern in terms of the amplitude of the perturbation.

Figure 3 shows the analytical observed velocity field with the aforementioned parameters. Despite its simplicity, the analytical model matches the shape of the different channels of the data. In particular, the bending of the isovelocity contours is described very well by the analytical model, especially in the blue-shifted region, where the effect of cloud contamination are negligible. The analytical models are produced using the publicly available code `GIGGLE`. It is important to point out that the model presented in Longarini et al. (2021) is limited to two dimensions and does not consider the vertical extent of the disc. There is evidence suggesting that the  $^{13}\text{CO}$  emission in Elias 2-27 is optically thick (Paneque-Carreño et al. 2022); consequently, the received signal does not originate from the midplane, but from a layer at  $z \neq 0$ . The analytical model we employ is not able to reproduce this effect, and, for a proper comparison, hydrodynamical and radiative transfer simulations would be needed. In any case, assuming that  $z/R < 0.3$  for the  $^{13}\text{CO}$  (Paneque-Carreño et al. 2022), the difference in inclination induced by the finite height of the emitting layer is  $\delta i = \arcsin(0.3) \simeq 0.29$ . The corresponding geometrical error is roughly  $1 - \sin(i + \delta i) / \sin(i) \simeq 15\%$ , that is subdominant compared to the one driven by the mass estimate.

### 3.4. Angular momentum transport and accretion

For a gravitationally unstable disc, kinematics offers a unique opportunity to quantify the transport of angular momentum of a gravitationally unstable disc. We show that gravitational instability in Elias 2-27 transports angular momentum and the equivalent  $\alpha$ -viscosity parameter is  $\alpha_{\text{GI}} = 0.038 \pm 0.018$ . Since the effective viscosity is responsible for the accretion process, it is

<sup>2</sup> The fitting procedure implemented in `SCIPY` returns an error for the best fit parameters. As for the  $\alpha_{\text{GI}}$  parameter, the error provided by the fit is subdominant compared to the one driven by the star and disc masses uncertainties.



**Fig. 2.** GI wiggle in the PV space: comparison between the the data (red line) and the model (blue line). The shaded region represents the error on the model, driven by the the uncertainties on the star and disc masses from Veronesi et al. (2021).

useful to predict the expected accretion rate onto the central object, and compare it to the observed one.

According to the self-similar solution (Lynden-Bell & Pringle 1974), the surface density and the accretion rate of the disc can be written as:

$$\Sigma = \frac{M_d}{2\pi R_c^2} \left(\frac{R}{R_c}\right)^{-1} \exp\left[-\frac{R}{R_c}\right], \quad (18)$$

$$\dot{M} = \frac{3M_d v_c}{2R_c^2} \exp\left[-\frac{R}{R_c}\right] \left(1 - \frac{2R}{R_c}\right), \quad (19)$$

where we have supposed that  $v = v_c(R/R_c)$ , where the subscript  $c$  means that the quantity is evaluated at the scale radius  $R_c$ . Within a  $\alpha$ -viscosity framework, the kinematic viscosity,  $\nu$ , is

$$\nu = \alpha c_s H = \alpha \left(\frac{H}{R}\right)^2 u_k R. \quad (20)$$

We note that within our assumption that  $T \propto R^{0.5}$ , for a constant  $\alpha$  the kinematic viscosity scales as  $\nu \propto R$ . In this way, we can write the accretion rate onto the central object as the limit for  $R \rightarrow 0$  of Eq. (19):

$$\dot{M}_\star = -\frac{3\alpha}{2} \left(\frac{H}{R}\right)_{R_c}^2 M_d \Omega_c, \quad (21)$$

where  $\Omega_c = \Omega(R_c) = \sqrt{GM_\star/R_c^3}$ .

Using  $\alpha_{\text{GI}} = 0.038$  and the disc parameters described in the previous paragraph, it is possible to compute the accretion rate onto the central object by using Eq. (21). Thus, we obtain:

$$\log_{10} \dot{M}_\star [\text{M}_\odot/\text{yr}] = -6.99 \pm 0.17, \quad (22)$$

where the error has been computed through propagation from the errors in  $\alpha_{\text{GI}}$ . The model for the accretion rate of Elias 2-27 reproduces the one measured by Natta et al. (2006) very well, namely,  $\log_{10} \dot{M}_\star [\text{M}_\odot/\text{yr}] = -7.2 \pm 0.5$ . They used J and K-band spectra to derive the mass accretion rate of objects in the

$\rho$ -Ophiuchi star forming region from the intensity of the hydrogen recombination lines. More recently, a new estimate of Elias 2-27 accretion rate was provided by [Testi et al. \(2022\)](#), being  $\log_{10} \dot{M}_\star [M_\odot/\text{yr}] = -7.3$ , which is consistent with the previous measurement.

To constrain  $\alpha_{\text{GI}}$  in Elias 2-27, we made the strong hypothesis that this quantity, or equivalently the cooling  $\beta$ , is constant throughout the disc. We are aware that, realistically, this is not the case. However, we point out that our disc model is self-consistent. Indeed, assuming a self-similar solution for the surface density with  $\Sigma \propto R^{-1}$ , we are imposing that the kinematic viscosity scales as  $\nu \propto R$ . Since  $\nu = \alpha c_s H$ , with  $c_s \propto R^{-0.25}$  ([Pérez et al. 2016](#)) and  $H \propto R^{1.25}$ , the viscosity coefficient,  $\alpha$ , should be constant with radius. We also point out that, in order to obtain an estimate of the amount of angular momentum transported within the disc from the GI wiggle, an assumption should be made with respect to how  $\alpha$  varies with the radius. A more realistic disc model for Elias 2-27 is not within the scope of this work. We stress that the choice of a self-similar profile for the surface density was made to maintain consistency with the work of [Veronesi et al. \(2021\)](#).

## 4. Discussion

The ability of our model to correctly reproduce the observed accretion rate points to the fact that gravitational instability is responsible for angular momentum transport in this system. As a matter of fact, the value of the  $\alpha$ -viscosity we get from the GI wiggle is the one required to explain the observed accretion rate onto the central object, having fixed the density structure of Elias 2-27. In addition, the strong hypothesis we made is that viscous processes are responsible for accretion. The inferred value for the  $\alpha$ -viscosity is higher than usually assumed ( $\sim 10^{-3} - 10^{-4}$ ). This is not surprising, since the strength of the viscosity generated by gravitoturbulent motions is higher than the expected in the non-self gravitating state ([Cossins et al. 2009](#)).

### 4.1. Infall and interaction with the environment

Elias 2-27 is a young system, and its interactions with the surrounding environment are possibly perturbing the disc. Specifically, the disc is partially embedded within the molecular cloud, which absorbs  $^{12}\text{CO}$  and a portion of the  $^{13}\text{CO}$  emission ([Pérez et al. 2016](#); [Paneque-Carreño et al. 2021](#)), then feeds the disc with mass. In particular, infall is an alternative way to trigger gravitational instability ([Kratte & Matzner 2006](#); [Kratte et al. 2008](#); [Kratte & Lodato 2016](#)). Gravitational instability occurs when the Toomre parameter is of the order of unity, and this threshold can be reached by cooling the disc (i.e. decreasing the sound speed) or by adding mass (i.e. increasing the surface density). When GI is triggered by infall, there is a mechanism akin to the thermal saturation ([Kratte & Lodato 2016](#)).

Our  $\alpha_{\text{GI}}$  estimate remains agnostic to the source of self-regulation, whether it arises from cooling or from the addition of mass to the disc. Indeed, what we are measuring through the wiggle is the amplitude of the surface density perturbation,  $\delta\Sigma/\Sigma$ . It is intrinsically linked to the efficiency of angular momentum that is transported by the spiral, regardless of the origin of the instability.

### 4.2. Planet formation in Elias 2-27

The value of  $\beta$  we measure is much higher than the threshold for disc fragmentation into bound gas clumps ([Gammie 2001](#); [Deng et al. 2017](#)), implying that (while the disc is gravitationally unstable) direct planet formation through gravitational instability is unlikely. However, many studies ([Paardekooper 2012](#); [Young & Clarke 2015](#)) showed that stochastic fragmentation of gas in spiral arms can happen for high values of  $\beta$ . As for the solid component, [Longarini et al. \(2023a,b\)](#); [Rowther et al. \(2024\)](#) investigated the possibility of forming planetary cores in gravitationally unstable discs through dust collapse. They found that for a sufficiently long cooling time,  $\beta > 10$ , and high disc-to-star mass ratio,  $M_d/M_\star \sim 0.2$ , dust efficiently collects inside spiral arms and its dispersion velocity is so low to induce collapse into bound objects with a mass of  $\sim 10M_\oplus$ . The inferred disc-to-star mass ratio ([Veronesi et al. 2021](#)) and the cooling time for Elias 2-27 make it a perfect candidate for planet formation through dust collapse.

[Huang et al. \(2018\)](#) characterised annular substructures in the discs within the DSHARP sample and found that Elias 2-27 has a gap at  $R_g = 69.1 \pm 0.4\text{au}$  with a width of  $\Delta = 14.3 \pm 1.1\text{au}$ . Although several mechanisms can explain the origin of gaps in protoplanetary discs, a common explanation is planet disc interaction. Under the planetary interpretation, the width of the gap scales as the Hill radius of the planet, defined as:

$$R_h = \left( \frac{M_p}{3M_\star} \right)^{1/3} R_g, \quad (23)$$

where  $M_p$  is the mass of the protoplanet. The last relation has been obtained by averaging results from hydrodynamical simulations. Following [Lodato et al. \(2019\)](#), the relation between the gap width and the Hill radius is  $\Delta = 5.5R_h$ , that translates into

$$M_p = 3 \left( \frac{\Delta}{5.5R_g} \right)^3 M_\star. \quad (24)$$

Using the gap width and location of [Huang et al. \(2018\)](#), and the star mass of [Veronesi et al. \(2021\)](#), the inferred mass of the protoplanet is  $M_p = 24 \pm 6M_\oplus$ . This result is in good agreement with the mass range of [Longarini et al. \(2023a,b\)](#). Another element that points towards the dust collapse is the value of the Toomre parameter. As shown in [Longarini et al. \(2023a\)](#), when the gravitational instability is driven by the cold component (dust in this case), the critical value of the Toomre parameter is  $> 1$ , as observed in Elias 2-27 (see Fig. 1).

## 5. Conclusion

In this work, we investigate the kinematic signatures of gravitational instability in the protoplanetary disc Elias 2-27. It is well known that gravitational instability leaves clear kinematic perturbations in molecular line emission ([Hall et al. 2020](#)) and their characteristics are related to the spiral density wave ([Longarini et al. 2021](#)). There are multiple arguments suggesting that Elias 2-27 is undergoing gravitational instability. Under the hypothesis that angular momentum is transported through the GI spirals, we estimate the  $\alpha$ -viscosity of the system, and link it to the accretion rate onto the central object. We find  $\alpha_{\text{GI}} = 0.038 \pm 0.018$  and  $\log_{10} \dot{M}_\star = -6.99 \pm 0.17M_\odot/\text{yr}$ . There is a very good agreement between the observed accretion rate and the one estimated from our model, pointing to the fact that gravitational instability is at play in this system and that is indeed driving angular

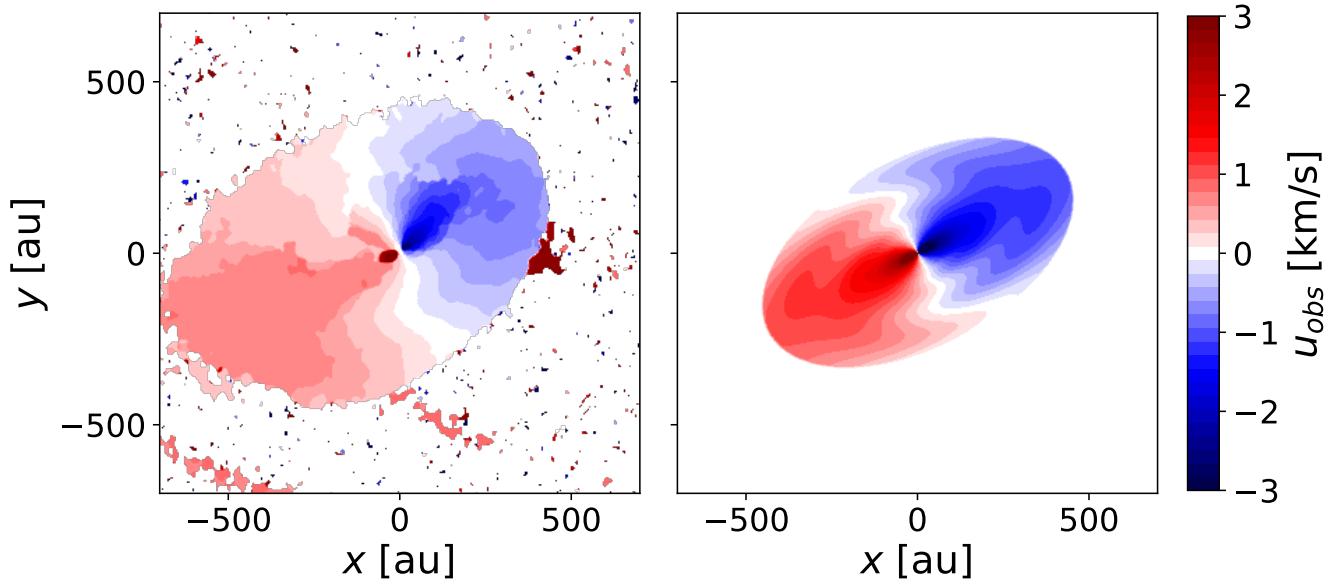


**Fig. 3.** Comparison between Elias 2-27 velocity map (left) and the best fit model for the velocity field with  $\alpha_{GI} = 0.038$  (right).

momentum transport. We underline that the results obtained in this work are valid assuming a disc model (as described in Sect. 3.3) and by fitting for the amplitude of the velocity perturbation in the central channel of the velocity map. The range of disc masses (Veronesi et al. 2021) and cooling factors inferred by our model makes Elias 2-27 a perfect candidate for dust collapse and the formation of planetary cores in spiral arms. The gap present in dust continuum emission at  $\sim 70$  au points to the presence of a  $\sim 20M_{\oplus}$  protoplanet, in agreement with the mass range of planets formed by collapse of the dust component by Longarini et al. (2023b).

*Acknowledgements.* This work has received funding from the European Union’s Horizon 2020 research and innovation programme under the Marie Skłodowska-Curie grant agreement # 823823 (RISE DUSTBUSTERS project). CL and CJC have been supported by the UK Science and Technology research Council (STFC) via the consolidated grant ST/W000997/1. PC acknowledges support by the Italian Ministero dell’Istruzione, Università e Ricerca through the grant Progetti Premiali 2012 – iALMA (CUP C52I13000140001). J.S. acknowledges financial support from the Natural Sciences and Engineering Research Council of Canada (NSERC) through the Canada Graduate Scholarships Doctoral (CGS D) program. The authors thank Francesco Zagaria, Andrew Sellek and Myriam Benisty for useful discussions.

## References

ALMA Partnership, Brogan, C. L., Pérez, L. M., et al. 2015, *ApJ*, 808, L3  
 Andrews, S. M., Huang, J., Pérez, L. M., et al. 2018, *ApJ*, 869, L41  
 Andrews, S. M., Wilner, D. J., Hughes, A. M., Qi, C., & Dullemond, C. P. 2009, *ApJ*, 700, 1502  
 Balbus, S. A. & Papaloizou, J. C. B. 1999, *ApJ*, 521, 650  
 Cossins, P., Lodato, G., & Clarke, C. J. 2009, *MNRAS*, 393, 1157  
 Deng, H., Mayer, L., & Meru, F. 2017, *ApJ*, 847, 43  
 Forgan, D., Rice, K., Cossins, P., & Lodato, G. 2011, *MNRAS*, 410, 994  
 Gaia Collaboration, Brown, A. G. A., Vallenari, A., et al. 2018, *A&A*, 616, A1  
 Gammie, C. F. 2001, *ApJ*, 553, 174  
 Hall, C., Dong, R., Teague, R., et al. 2020, *ApJ*, 904, 148  
 Hall, C., Rice, K., Dipierro, G., et al. 2018, *MNRAS*, 477, 1004  
 Hennebelle, P., Lesur, G., & Fromang, S. 2017, *A&A*, 599, A86  
 Huang, J., Andrews, S. M., Pérez, L. M., et al. 2018, *ApJ*, 869, L43  
 Kratter, K. & Lodato, G. 2016, *ARA&A*, 54, 271  
 Kratter, K. M. & Matzner, C. D. 2006, *MNRAS*, 373, 1563

Kratter, K. M., Matzner, C. D., & Krumholz, M. R. 2008, *ApJ*, 681, 375  
 Law, C. J., Teague, R., Loomis, R. A., et al. 2021, *ApJS*, 257, 4  
 Lee, C.-F., Li, Z.-Y., & Turner, N. J. 2020, *Nature Astronomy*, 4, 142  
 Lesur, G., Hennebelle, P., & Fromang, S. 2015, *A&A*, 582, L9  
 Lodato, G., Dipierro, G., Ragusa, E., et al. 2019, *MNRAS*, 486, 453  
 Lodato, G. & Rice, W. K. M. 2004, *MNRAS*, 351, 630  
 Lodato, G. & Rice, W. K. M. 2005, *MNRAS*, 358, 1489  
 Longarini, C., Armitage, P. J., Lodato, G., Price, D. J., & Ceppi, S. 2023a, *MNRAS*, 522, 6217  
 Longarini, C., Lodato, G., Bertin, G., & Armitage, P. J. 2023b, *MNRAS*, 519, 2017  
 Longarini, C., Lodato, G., Toci, C., et al. 2021, *ApJ*, 920, L41  
 Lynden-Bell, D. & Kalnajs, A. J. 1972, *MNRAS*, 157, 1  
 Lynden-Bell, D. & Pringle, J. E. 1974, *MNRAS*, 168, 603  
 Manara, C. F., Ansdell, M., Rosotti, G. P., et al. 2023, in *Astronomical Society of the Pacific Conference Series*, Vol. 534, *Protostars and Planets VII*, ed. S. Inutsuka, Y. Aikawa, T. Muto, K. Tomida, & M. Tamura, 539  
 Meru, F., Juhász, A., Ilee, J. D., et al. 2017, *ApJ*, 839, L24  
 Natta, A., Testi, L., & Randich, S. 2006, *A&A*, 452, 245  
 Paardekooper, S.-J. 2012, *MNRAS*, 421, 3286  
 Paneque-Carreño, T., Miotello, A., van Dishoeck, E. F., et al. 2022, *A&A*, 666, A168  
 Paneque-Carreño, T., Pérez, L. M., Benisty, M., et al. 2021, *ApJ*, 914, 88  
 Pinte, C., Price, D. J., Ménard, F., et al. 2020, *ApJ*, 890, L9  
 Pérez, L. M., Carpenter, J. M., Andrews, S. M., et al. 2016, *Science*, 353, 1519  
 Rowther, S., Nealon, R., Meru, F., et al. 2024, *MNRAS*, 528, 2490  
 Segura-Cox, D. M., Schmiedecke, A., Pineda, J. E., et al. 2020, *Nature*, 586, 228  
 Shakura, N. I. & Sunyaev, R. A. 1973, *A&A*, 24, 337  
 Sheehan, P. D. & Eisner, J. A. 2018, *ApJ*, 857, 18  
 Shu, F. H. 1970, *ApJ*, 160, 99  
 Speedie, J., Dong, R., & Hall, C. e. 2024, submitted, *Nature*, 2, 2  
 Teague, R. 2019, *Research Notes of the American Astronomical Society*, 3, 74  
 Teague, R. & Foreman-Mackey, D. 2018, *Research Notes of the American Astronomical Society*, 2, 173  
 Terry, J. P., Hall, C., Longarini, C., et al. 2022, *MNRAS*, 510, 1671  
 Testi, L., Natta, A., Manara, C. F., et al. 2022, *A&A*, 663, A98  
 Tobin, J. J., Sheehan, P. D., Megeath, S. T., et al. 2020, *ApJ*, 890, 130  
 Toomre, A. 1969, *ApJ*, 158, 899  
 Veronesi, B., Paneque-Carreño, T., Lodato, G., et al. 2021, *ApJ*, 914, L27  
 Virtanen, P., Gommers, R., Oliphant, T. E., et al. 2020, *Nature Methods*, 17, 261  
 Young, M. D. & Clarke, C. J. 2015, *MNRAS*, 451, 3987